ISSN 1063-7761, Journal of Experimental and Theoretical Physics, 2007, Vol. 105, No. 5, pp. 909–915. © Pleiades Publishing, Inc., 2007.
Original Russian Text © S.S. Kharintsev, G.G. Hoffmann, J. Loos, G. de With, P.S. Dorozhkin, M.Kh. Salakhov, 2007, published in Zhurnal Éksperimental'noĭ i Teoreticheskoĭ Fiziki, 2007, Vol. 132, No. 5, pp. 1044–1051.

ATOMS, MOLECULES, OPTICS

Subwavelength-Resolution Near-Field Raman Spectroscopy

S. S. Kharintsev[a, b, *], G. G. Hoffmann[b, c], J. Loos[b], G. de With[b], P. S. Dorozhkin[d], and M. Kh. Salakhov[a]

[a] *Kazan State University, Kazan, 420008 Russia*
[b] *Eindhoven University of Technology, PO Box 513, 5600 MB, Eindhoven, The Netherlands*
[c] *University of Duisburg-Essen, D-45117, Essen, Germany*
[d] *Institute of Solid-State Physics, Russian Academy of Sciences, Chernogolovka, Moscow oblast, 142432 Russia*
**e-mail: red@ksu.ru*

Received April 10, 2007

Abstract—The resolution capabilities of near-field Raman spectroscopy based on a giant enhancement of the electric field near a nanosized metal probe are studied. As a test sample, bundles of single-walled carbon nanotubes deposited on glass substrates are used. It is shown that this method ensures a subwavelength spatial resolution of about 50 nm and demonstrates a Raman scattering enhancement of the order of 10^4.

PACS numbers: 42.62.Fi, 42.65.-k, 42.65.An

DOI: 10.1134/S1063776107110052

1. INTRODUCTION

Optical spectroscopy methods are of fundamental importance in studying the structure and properties of matter. However, due to the well-known Abbe diffraction limit, which is about $\lambda/2n$ (λ is the wavelength of radiation and n is the refractive index), these methods cannot be applied to study objects with a subwavelength resolution. The existing methods for the improvement of the spatial resolution in the visible range (for example, frequency mixing, second-harmonic generation, etc.) do not suffice to study nanostructures.

The occurrence of evanescent waves in the near-field region (not farther than 100 nm from the interface between two media) makes it possible to overcome the diffraction limit and, therefore, to achieve ultrahigh resolution in optical spectroscopy [1–3]. It has become possible to practically implement this approach by combining two methods, optical spectroscopy and scanning probe microscopy [1–5]. A key role in this method is played by a nanosized probe placed near the surface (at ~3 nm) of a sample under investigation. Unlike traditional optical spectroscopy, the resolving power is determined by the geometry of a probe rather than by the aperture of optical elements. Therefore, for this very reason, this method is often referred to as apertureless near-field optical microscopy [1–5]. With respect to the principle of formation of the optical image, local scattering-based and local excitation-based methods are commonly used [4]. In the first case, the evanescent field near nanosized structures is scattered by a probe and is measured in the far-field region by "ordinary" optics. In the second case, a probe placed in a tightly focused laser beam locally enhances the electromagnetic field near its tip due to the resonance excitation of localized surface plasmons. An additional contribution to the field enhancement is made by a geometric singularity of the tip apex and by the chemical effect of adsorbed molecules [4–7]. The enhanced field is scattered from nanosized structures and is detected in the far-field region. In the general case, the optical image in the far field is a result of the combined action of the above effects (the interference of different contributions); therefore, interpreting the measurement results can be challenging.

In contrast to widely used methods of electron microscopy, the approach considered makes it possible not only to visualize the object of interest, but also to in situ obtain information on its chemical structure, composition, and conformational state on the nanoscale. In connection with this, the method of near-field Raman spectroscopy is developing vigorously [4, 5, 8–14].

The objective of this study is to demonstrate a giant enhancement of the electromagnetic field and an ultrahigh spatial resolution of the method of near-field Raman spectroscopy using single-walled carbon nanotubes as an example. The choice of these objects is determined by the fact that a nanotube is an ideal quasi-one-dimensional tubular graphite structure 0.5–3.0 nm in diameter and a few micrometers long. At the same time, the Raman spectrum of carbon nanotubes is well studied; it consists of strong spectral lines attributed to the normal modes of the graphite lattice. It is important to note that the observation of the Raman spectrum from one single nanotube is possible because its density of electronic states is very high, being close in magnitude to van Hove singularities [15–17]. Resonance Raman scattering makes it possible to extract information on the structure of a nanotube by identifying the

atomic coordinates of the unit cell (*n, m*). By studying the parameters of spectral lines, we can determine such parameters of nanostructures as their diameter, chirality, excitation energy, local defects, and so on [18, 19].

2. THEORY

The excitation of resonance plasmons in metal structures plays a fundamental role in near-field optical spectroscopy [1–5]. The problem of scattering of electromagnetic radiation from spherical subwavelength particles has been analytically solved by Mie [20]. In the quasistatic limit, the solution of Maxwell's equations for a spherical metal probe in a uniform external field E_0 yields the following expressions for the electric fields inside and outside the metal sphere, $\mathbf{E}_{in}$ and $\mathbf{E}_{out}$ [1]:

$$\mathbf{E}_{in} = \frac{2\varepsilon_m}{\varepsilon_{tip} + 2\varepsilon_m} E_0 \mathbf{e}_z, \quad (1)$$

$$\mathbf{E}_{out} = E_0 \mathbf{e}_z + \frac{\varepsilon_{tip} - \varepsilon_m}{\varepsilon_{tip} + 2\varepsilon_m} \times \frac{R^3}{r^3} E_0 (2\mathbf{e}_r \cos\theta + \mathbf{e}_\theta \sin\theta). \quad (2)$$

Here, $\mathbf{e}_z$, $\mathbf{e}_\theta$, and $\mathbf{e}_r$ are the unit vectors; R is the radius of the sphere; and ε_{tip} and ε_m are the permittivities of the sphere and surrounding medium, respectively. The scattered field is described by the second term in Eq. (2) and is equivalent to the field of a dipole moment placed at the center of the sphere,

$$\mathbf{p} = \alpha \varepsilon_m \mathbf{E}_0, \quad (3)$$

where

$$\alpha = 4\pi R^3 \frac{\varepsilon_{tip} - \varepsilon_m}{\varepsilon_{tip} + 2\varepsilon_m} \quad (4)$$

is the polarizability of the sphere. It follows from Eq. (4) that, if the resonance condition

$$\varepsilon_{tip} = -2\varepsilon_m \quad (5)$$

is satisfied, the polarizability becomes singular, and the field emitted by the dipole is enhanced. Based on expression (4) for the polarizability, one can obtain the following expressions for the scattering and absorption cross sections in the far-field region [1]:

$$C_{sc} = \frac{k^4}{6\pi} |\alpha|^2 \text{ and } C_{abs} = k \text{Im}\alpha. \quad (6)$$

There is an additional component of the electric field near the metal sphere, which does not propagate (its Poynting vector is zero). By integrating the electric field strength over the sphere surface, we obtain an expression for the near-field scattering cross section [1] as a function of the particle size,

$$C_{near}(R) = \frac{\alpha^2}{6\pi} \left(\frac{3}{R^4} + \frac{k^2}{R^2} + k^4 \right). \quad (7)$$

It follows from Eq. (5) that the permittivity of the material of a probe plays a central role in implementing the resonance condition in the dipole approximation. There are two contributions in the permittivity of metals. One of them is related to free electrons, $\varepsilon_e(\omega)$, whereas the other contribution arises due to interband transitions, $\varepsilon_{ib}(\omega)$. Within the framework of the Drude model of free electrons [1], the permittivity can be written as a sum of two components,

$$\varepsilon(\omega) = \varepsilon_e(\omega) + \varepsilon_{ib}(\omega) = 1 - \frac{\omega_p^2}{\omega^2 + i\Gamma_{bulk}\omega} + \varepsilon_{ib}(\omega), \quad (8)$$

where

$$\omega_p = \left(\frac{ne^2}{\varepsilon_0 m_e} \right)^{1/2}$$

is the plasma frequency, and Γ_{bulk} is the damping constant.

If the size R of a metal particle is smaller than the electron free path l_e (electrons predominantly collide with particle boundaries), the particle permittivity becomes the function of the particle size, and the expression for this quantity differs from that given by formula (8). To taken into account this effect, it is necessary to change the damping constant as follows [1]:

$$\Gamma = \Gamma_{bulk} + \frac{A v_F}{R}, \quad (9)$$

where R is the linear particle size, v_F is the Fermi velocity, and A is a constant that takes into consideration the particle shape. For example, for silver, $\text{Im}\varepsilon(\omega) = 0.23 + 2.64/R$ ($\lambda_{exc} = 488$ nm) [13].

The transitions $3d \longrightarrow 4sp$, $4d \longrightarrow 5sp$, and $5d \longrightarrow 6sp$ are the key transitions for copper, silver, and gold; in this case, free electrons are in the 4*s*, 5*s*, and 6*s* states, respectively. The advantage of the use of nanoprobes from these metals in optical measurements is that the plasmon resonances of copper, silver, and gold lie in the visible spectral range [1–5]. Furthermore, it is necessary to take into account that the permittivity of a metal depends on the wavelength of excitation radiation. For example, for gold, $\varepsilon = -2.2 + 3.8i$ ($\lambda_{exc} = 488$ nm), $\varepsilon = -6.3 + 2.0i$ ($\lambda_{exc} = 540$ nm), and $\varepsilon = -25 + 1.5i$ ($\lambda_{exc} = 800$ nm) [4]. Therefore, the near-IR range is optimal for the excitation of plasmons in gold.

The basic characteristics of near-field optical spectroscopy are the enhancement factor of the electric field and the spatial resolution. The latter parameter is determined by the radius of curvature of the apex of the probe tip and can reach a few nanometers. At present, there are several approaches to estimate the enhancement effect of the electric field in the near-field region

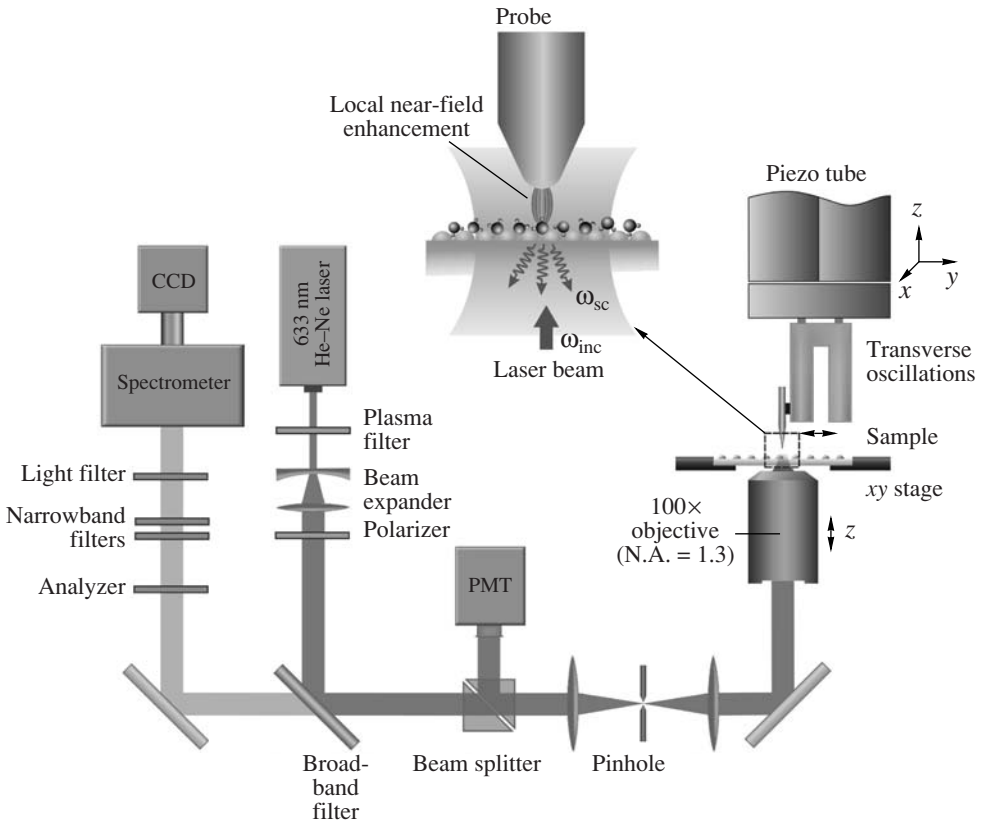

Fig. 1. Optical layout of a scanning near-field nanoscope.

[2]. To identify the plasmon effect and to estimate the enhancement that it causes, we propose to use the following relation:

$$F = \frac{(I_{\text{near}} - B_{\text{near}}) - (I_{\text{far}} - B_{\text{far}})}{I_{\text{far}} - B_{\text{far}}} \frac{d_{\text{spot}}^2}{d_{\text{tip}}^2}, \qquad (10)$$

where I_{near}, B_{near}, I_{far}, and B_{far} are the intensities and backgrounds in the near-field (the probe is brought close to the sample) and in the far-field (the probe is moved away from the sample) regions, respectively; d_{spot} is the size of the laser spot (~λ); and d_{tip} is the size of the near-field interaction zone ($d_{\text{tip}} = \sqrt{2Rh}$, h is the distance between the probe and the sample [21]). It is necessary to emphasize that estimate (10) is rough, because it does not take into account many effects (occurring in nanosized structures), which are connected with the Landau damping, the geometric configuration of the probe, the excitation wavelength, and the polarization.

3. EXPERIMENTAL SETUP

Figure 1 shows the optical layout of an NTEGRA Spectra near-field optical nanoscope (NT-MDT, Russia), which was used in our experiments. A linearly polarized laser beam (632.8 nm) passes through a plasma filter and a beam expander, reflects off of a broadband filter and is directed through a beam splitter and a pinhole to an inverted optical microscope. A 100-fold immersion objective with the numerical aperture N.A. = 1.3 focuses the laser beam into a spot with a diameter smaller than 300 nm. The probe is controlled by a shear-force feedback mechanism and is maintained, on the average, at a height of 3 nm from the sample surface. A near-field image of the object under study is formed by a raster scanning the object with an *xy* stage, retaining fixed the position of the probe with respect to the laser spot. The scattered and reflected light is collected by the same objective and is directed backward along the same optical path. The light passes through the pinhole and beam splitter and is detected by a photomultiplier. The remaining part of this light beam passes through the broadband filters, the system of narrowband filters, and a light filter and is detected with a thermally cooled CCD matrix. All the Raman spectra were measured in the range 150–3000 cm^{-1} with a spectral resolution of about 15 cm^{-1}. The signal acquisition time was 500 ms per pixel; the power on the sample amounted to 100 μV. With this experimental setup, it is possible to measure (i) the topography, the phase contrast, etc., in the atomic-force and shear-force microscopy modes, (ii) the confocal optical image, (iii) the

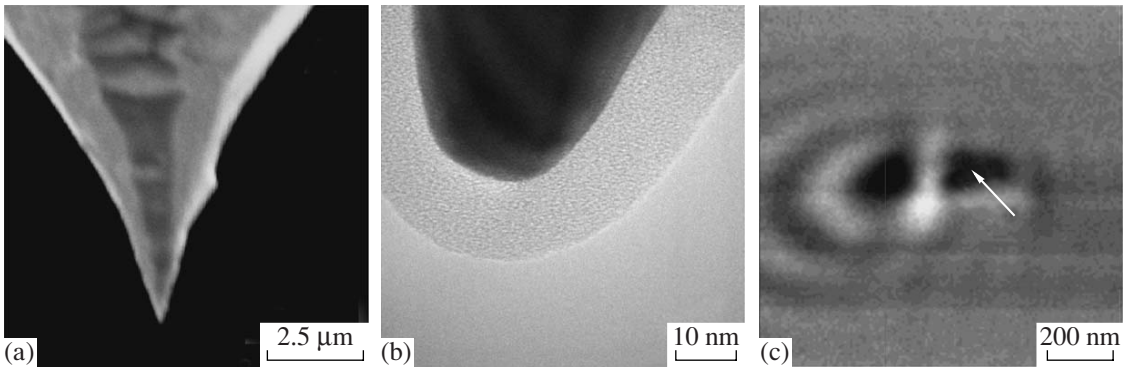

Fig. 2. Images of (a) a probe and (b) the apex of its tip obtained, respectively, with a scanning electron microscope and a high-resolution transmission electron microscope and (c) confocal optical image of a probe upon its scanning along a glass surface.

Raman spectrum and the Raman image (including fluorescence), and (iv) the probe-enhanced Raman spectrum and the Raman image (fluorescence enhancement/quenching).

4. RESULTS AND DISCUSSION

To demonstrate that it is possible to obtain a giant enhancement of the electric field and a subwavelength spatial resolution with a near-field optical nanoscope (see Fig. 3 below), we used single-walled carbon nanotubes (HiPCo, Carbon Nanotechnology Inc.). These tubes are quasi-one-dimensional structures, which exhibit strong characteristic Raman lines. To prepare the sample, 0.05 g of carbon nanotube powder was mixed with 20 g of dichloromethane, and the mixture was sonicated at 20 W within 60 min at 0°C. A thin film was deposited on a coverslip by centrifuging the dispersion obtained at a rate of 300 rpm within 120 s.

Probes used in experiments were prepared by electrochemical etching of a 99.999% pure gold wire in a 1 : 1 solution of HCl (37%) and C_2H_5OH at a constant voltage of 2.4 V [22]. Figures 2a and 2b show the general view of a probe tip and its apex, which were obtained, respectively, with a JSM-840A (JEOL) scanning electron microscope operated at 10 kV, and a Tecnai G2 20 transmission electron microscope operated at 200 kV. As is seen from Fig. 2, the radius of the apex of the probe tip is approximately equal to 14 nm. The occurrence of a uniform shell around the tip apex results from carbon contamination in the chamber of the scanning electron microscope. The effect of this shell on the electromagnetic field enhancement has yet to be studied.

To enhance the electric field with the help of the plasmon effect, the laser light should be polarized parallel to the probe axis (the *p*-polarization). However, in the inverted configuration (see Fig. 1), this condition does not hold, because the direction of polarization is perpendicular to the probe axis (the *s*-polarization). Nevertheless, surface plasmons can be resonantly excited due to the occurrence of a longitudinal component of the electromagnetic field at the periphery of the waist of the tightly focused laser beam (the Gaussian TEM_{00} mode) [23, 24]. A confocal optical image of the probe upon its scanning along the glass surface (see Fig. 2c) demonstrates the occurrence of two minima located along the direction of polarization, which correspond to the resonance absorption of the energy of the incident light wave. In this case, the charge density on the probe surface, oscillating at the same frequency as the excitation field, is distributed symmetrically with respect to the tip apex; as a result, a constructive interference pattern of the electric field arises on this surface. Therefore, for the plasmon effect to be maximal, the metal probe should be placed at one of the two minima located at the periphery of the laser spot. Because the probe can be oriented at some angle to the optical axis and/or be asymmetric in shape, the energy is absorbed nonuniformly, and, therefore, the magnitude of the enhancement created by the probe depends on the choice of the minimum. In our case, the maximal enhancement of the signal was achieved for the minimum indicated by the arrow in Fig. 2c.

It is important to note that the intensity of the longitudinal component of the field is approximately five times lower than the intensity of the transverse component at the center of the beam. To enhance the longitudinal component, it is necessary to use higher-order laser modes, for example, a Gauss–Hermite beam, TEM_{10}, [23]. It was shown in [23, 24] that, in the radially polarized laser light, the intensity of the longitudinal component at the center of the beam is two times higher compared to the transverse component.

The Raman spectrum of carbon nanotubes exhibits five characteristic modes [18, 19]. The radial breathing mode (*RBM*) lies in the range (100–300 cm^{-1}); the *D* line is peaked at ~1310 cm^{-1}; its first overtone *D** is located at ~2606 cm^{-1}; and the G^+ and G^- lines are located near 1587 and 1559 cm^{-1}, respectively. Based on an analysis of the *RBM* mode, one can determine the diameter of a nanotube (carbon atoms execute radial vibrations), its structure (*n*, *m*), and, correspondingly, its chirality. The *G* line yields information on whether a

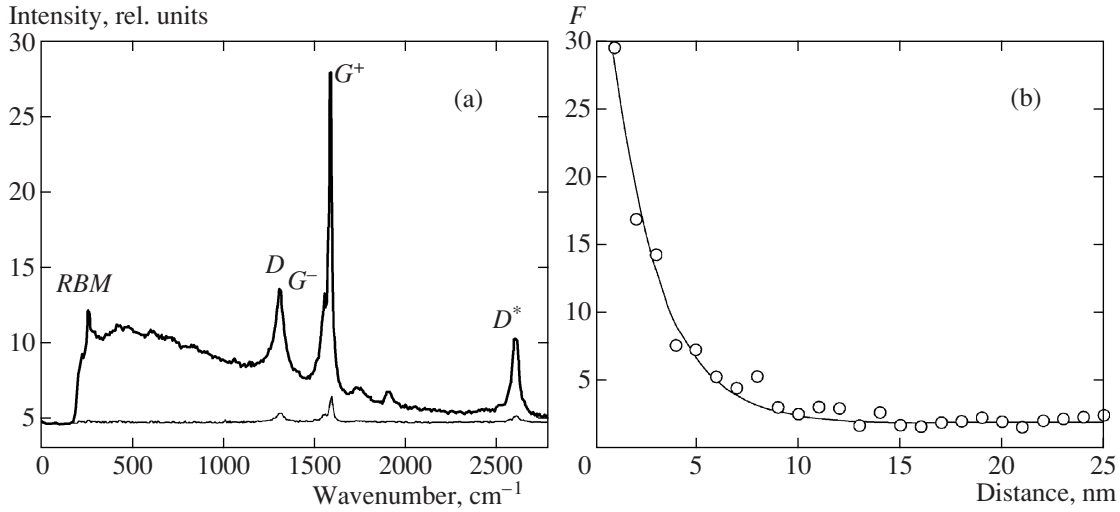

Fig. 3. (a) Raman spectra of carbon nanotubes in the presence (the thin curve) and absence (the thick curve) of the interaction of the probe with the sample; (b) spectral line intensity ($\Delta\nu = 1594$ cm^{-1}) in relation to the distance between the probe and the sample.

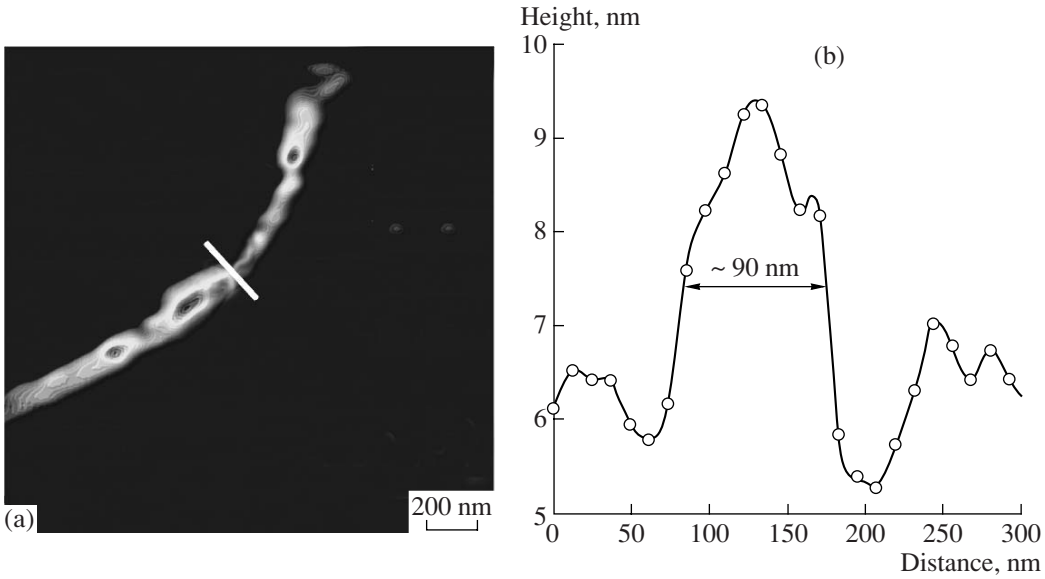

Fig. 4. (a) Atomic-force image of the bundle of nanotubes and (b) its cross section along the white line.

nanotube is of the metal or semimetal type. The difference G^+–G^- allows the nanotube diameter to be determined because the G^- vibration is caused by tangent motions of carbon atoms perpendicular to the nanotube axis. Structural defects and irregularities determine the parameters of the D line and its first overtone D^*.

The Raman spectra of carbon nanotubes obtained using the probe and recorded in the shear-force microscopy mode are shown in Fig. 3. The enhancement factor estimated by formula (10) from these data for each of the five modes considered above was found to be ~9750 (*RBM*), ~7500 (D line), ~9750 (D^* line), ~9000 (G^+ line), and ~10500 (G^- line). Therefore, the signal enhancement is nonuniform for different modes. A slight background observed in the range 200–2000 cm^{-1} is caused by the light reflected from the probe.

Figure 4 shows the topographic pattern of the bundle of carbon nanotubes deposited on a glass coverslip and its cross section along the white solid line that were obtained with the help of an atomic-force microscope. As is seen from this figure, the lateral resolution, which is determined by the convolution of the tip apex and the structure of the bundle, is about 90 nm. Judging from the height of the cross section, one can assume that this bundle consists of at least two to three nanotubes. The same follows from the complex structure of the *RBM* line (~258 cm^{-1}) (see Fig. 3), from which we unambig-

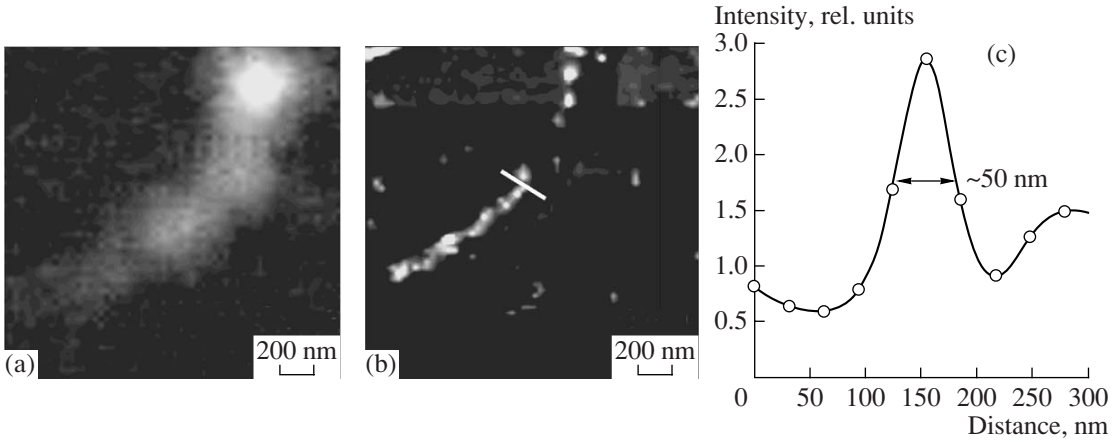

Fig. 5. (a) Confocal optical and (b) near-field Raman ($\Delta\nu = 258$ cm^{-1}) images of the bundle of nanotubes; (c) image cross section along the white line.

uously identify the number and the diameter of nanotubes, $d = 0.9 \pm 0.2$ nm. Figure 5 presents the confocal Raman images (the *RBM* mode, $\Delta\nu = 258$ cm^{-1}) of the bundle of nanotubes shown in Fig. 4a that were obtained without (Fig. 5a) and with (Fig. 5b) using the probe. As should be expected, the spatial resolution in the first case is restricted by the diffraction limit, which is approximately equal to 300 nm. In the second case, the spatial resolution is estimated by the profile FWHM, which yields about 50 nm (see Fig. 5c). Therefore, near-field Raman spectroscopy improves fivefold the spatial resolution compared to confocal optical microscopy. Comparison of Figs. 4 and 5 shows that the topographic and near-field Raman images strongly correlate with each other. However, the intensity distribution along the bundle of nanotubes does not correlate with the topographic pattern. This can be explained by the fact that nanotubes are differently interlaced with each other and form a bundle composed of nanotubes of different diameters. At the same time, the resonance condition for the excitation wavelength (λ_{exc} = 632.8 nm) can be violated along the nanotube length. Hence, near-field Raman spectroscopy makes it possible to avoid the averaging of the Raman spectrum over the entire bundle of nanotubes and ensures the possibility of local studying its structure with an ultrahigh resolution.

CONCLUSIONS

By achieving a spatial resolution of about 50 nm and obtaining an enhancement of the Raman signal of the order of 10^4, we demonstrated the potentialities of near-field Raman spectroscopy, which is based on the giant enhancement of the electric field near a nanosized probe. Therefore, this method is an efficient tool for local nondestructive chemical analysis of substance on the nano and/or submicron scale. Despite that, presently, many researches have been capable of achieving similar results, it is still too early to state that this method can be used in routine analysis (for example, in considering applied chemical or biological problems). First of all, this is connected with the multiparametric character of this method. The greatest difficulty is to take into account the influence of the probe shape and size on the enhancement of the Raman signal. Therefore, an important problem of near-field Raman spectroscopy is to study the influence of the probe geometry on plasmon effects in various media.

REFERENCES

1. *Nano-Optics*, Ed. by S. Kawata, M. Ohtsu, and M. Irie (Springer, Berlin, 2002).
2. P. N. Prasad, *Nanophotonics* (Wiley, Hoboken, N.J., 2004).
3. D. Courjon, *Near-Field Microscopy and Near-Field Optics* (Imperial College Press, London, 2003).
4. L. Novotny and S. J. Stranick, Annu. Rev. Phys. Chem. **57**, 303 (2006).
5. A. Hartschuh, M. R. Beversluis, A. Bouhelier, et al., Philos. Trans. R. Soc. London, Ser. A **362**, 807 (2004).
6. A. Campion and P. Kambhampati, Chem. Soc. Rev. **27**, 241 (1998).
7. Z. Q. Tian, J. Raman Spectrosc. **36**, 466 (2005).
8. C. Vannier, B. Yeo, J. Melanson, and R. Zenobi, Rev. Sci. Instrum. **77**, 023104 (2006).
9. F. Zenhausern, M. P. O'Boyle, and H. K. Wickramasinghea, Appl. Phys. Lett. **65**, 1623 (1994).
10. G. P. Gucciardi, S. Trusso, C. Vasi, et al., Appl. Opt. **42**, 2724 (2003).
11. W. X. Sun and Z. X. Shen, J. Raman Spectrosc. **34**, 668 (2003).
12. D. Bulgarevich and M. Futamata, Appl. Spectrosc. **58**, 757 (2004).
13. D. Richards, R. G. Milner, F. Huang, et al., J. Raman Spectrosc. **34**, 663 (2003).

14. B. Pettinger, B. Ren, G. Picardi, et al., J. Raman Spectrosc. **36**, 541 (2005).
15. M. A. Pimenta, A. Marucci, S. D. Brown, et al., J. Mater. Res. **13**, 2396 (1998).
16. A. G. Souza Filho, A. Jorio, G. G. Samsonidze, et al., Nanotechnology **14**, 1130 (2003).
17. C. Jiang, J. Zhao, H. A. Therese, et al., J. Phys. Chem. **107**, 8742 (2003).
18. N. Hayazawa, T. Yano, H. Watanabe, et al., Chem. Phys. Lett. **376**, 174 (2003).
19. N. Anderson, P. Anger, A. Hartschuh, and L. Novotny, Nanoletters **6**, 744 (2006).
20. G. Mie, Ann. Phys. (Leipzig) **25**, 377 (1908).
21. V. N. Konopsky, K. E. Kouyanov, and N. N. Novikova, Ultramicroscopy **88**, 127 (2001).
22. B. Ren, G. Picardi, and B. Pettinger, Rev. Sci. Instrum. **75**, 837 (2004).
23. L. Novotny, M. R. Beversluis, and K. S. Youngworth, Phys. Rev. Lett. **86**, 5251 (2001).
24. A. Bouhelier, M. R. Beversluis, and L. Novotny, Appl. Phys. Lett. **82**, 4596 (2003).

Translated by V. Rogovoĭ